X-621-71-57
PREPRINT

NASA TM X- 65462

THE RESPONSE OF THE THERMOSPHERIC DENSITY TO AURORAL HEATING DURING GEOMAGNETIC DISTURBANCES

H. VOLLAND
H.G. MAYR

JANUARY 1971

GSFC
GODDARD SPACE FLIGHT CENTER
GREENBELT, MARYLAND

X-621-71-57

THE RESPONSE OF THE THERMOSPHERIC DENSITY TO AURORAL HEATING DURING GEOMAGNETIC DISTURBANCES

by

H. Volland† and H. G. Mayr‡

January 1971

† Astronomical Institutes of the University, Bonn, Germany
‡ NASA Goddard Space Flight Center, Greenbelt, Md., USA

Goddard Space Flight Center

Greenbelt, Maryland

THE RESPONSE OF THE THERMOSPHERIC DENSITY TO AURORAL HEATING DURING GEOMAGNETIC DISTURBANCE

H. Volland and H. G. Mayr

ABSTRACT

Assuming an impulse type heat input into a small band of latitude within the aurora ovals during local night; which shall simulate a heat input during geomagnetic disturbances, the corresponding response of the thermospheric density has been calculated. The result in terms of a series of spherical harmonics shows that the components with large wave domain numbers (n, m) decay rapidly within the first hour after the onset of the geomagnetic storm while the two zonal components (0, 0) and (2, 0) and the two associated components (1, 1) and (3, 1) are predominant during the slow tail phase of the disturbance. It is that slow tail of the density disturbance beginning about one hour after the onset of the storm which contains most of the spectral energy and which is responsible for the observed world wide response of the thermospheric density during geomagnetic storms. Its dependence on storm time, latitude and longitude is discussed and compared with available satellite drag data.

CONTENTS

		Page
	ABSTRACT	iii
1.	INTRODUCTION	1
2.	THE DISTRIBUTION OF THE HEAT INPUT	2
3.	THE THERMOSPHERE SYSTEM TRANSFER FUNCTION	5
4.	THE DENSITY RESPONSE AS FUNCTION OF TIME	13
	4.1 The Zonal Components	14
	4.2 The Local Time Dependence of the Density Disturbance	19
5.	DISCUSSION AND CONCLUSION	21
6.	LITERATURE	24
	FIGURE CAPTION	27

THE RESPONSE OF THE THERMOSPHERIC DENSITY TO AURORAL HEATING DURING GEOMAGNETIC DISTURBANCES

1. INTRODUCTION

During geomagnetic disturbances the thermospheric density increases (Jacchia, 1959), at least between 160 and 1000 km altitude (Jacchia et al. 1967). We shall refer to this phenomenon as "geomagnetic activity effect" of the thermospheric density. According to Jacchia and Slowey (1964a; 1964b), the intensity of the geomagnetic activity effect is proportional to the planetary index a_p for large disturbances and is proportional to the index K_p for small disturbances. The effect occurs on a world wide basis. But the density disturbance appears to be systematically larger at high latitudes and during local midnight than at the equator during local noon (Roemer, 1970). The time lag between the peak of the geomagnetic disturbance and the corresponding density increase is about 5 to 7 hours at low latitudes. That time lag is shorter by about one or two nours at high latitudes than at the equator (Jacchia et al, 1967). Tne density disturbance has an impulse form with a typical pulse width of one day.

Thomas and Cning (1969) and Volland (1969) applying a simple one dimensional vertical model reproduced the height profile and the mean time lag of the density disturbance and concluded that the heat input responsible for the geomagnetic activity effect occurs predominantly within the lower thermospheric between 100 and 200 km altitude and that the time delay is the natural response of the thermosphere to a pulse type disturbance of the heat input.

From the observations as well as from theory it is obivous that the most likely heating mechanisms of the geomagnetic activity effect are due to the penetration of high energetic charged particles into the aurora ovals thus ionizing the neutral gas within a small band near ±65° geographic latitude, and energy transfer into heat of the neutral thermosphere via Joule heating (Cole, 1970) and recombination processes. These heating mechanisms are of course rather local phenomena. Therefore, the questions arise how the heat is transfered from the auroral regions to lower latitudes and why the response of the thermospheric density is worldwide in spite of the local heat input. We shall attempt to answer these questions in this paper with the help of a three dimensional thermospheric model.

2. THE DISTRIBUTION OF THE HEAT INPUT

During periods of enhanced solar activity, fast ionized particles can penetrate from the magnetosphere into the aurora ovals, predominantly on the night time hemisphere (Akasofu, 1968). Tney react with the neutral gas mainly in the height range between 100 and 200 km and cause auroras and polar electro jets. We expect that the corresponding heating of the thermosphere occurs just in those ranges of height and geographic location during geomagnetic storms.

Since the problem we are concerned here with is rather complicated we want to select a model which is as simple as possible. We therefore assume that the heating process is limited to a narrow band at ±65° geographic latitude on the night time hemisphere during equinox and we neglect the inclination of the geomagnetic dipole with respect to the geographic axis:

$$\Delta Q \begin{cases} \Delta Q_0 \, f(t) \, g(z) & \varphi_0 < |\varphi| < \varphi_0 + \Delta\varphi \\ & \text{for} \quad |\tau| < \pi/2 \\ 0 & \text{otherwise.} \end{cases} \tag{1}$$

Here is ΔQ_0 (in erg/cm^3 sec) a constant heat input at an altitude of $z_0 \approx 100$ km within the strip between φ_0 and $\varphi_0 + \Delta\varphi$ latitude, τ is the local time (zero at local midnight). For conveniance we assume very simple structures for the height distribution and the time variation of the disturbance:

$$g(z) \begin{cases} \exp(-(z - z_0)/H) & z > z_0 \approx 100 \text{ km} \\ & \text{for} \\ 0 & z < z_0, \end{cases} \tag{2}$$

where z is the height above ground and H is a constant scale height, and

$$f(t) \begin{cases} \exp(-a\,t) & t > 0 \\ & \text{for} \\ 0 & t < 0, \end{cases} \tag{3}$$

where t is the storm time and is a constant decay factor.

As it is well known (Chapman and Bartels, 1951) each regular function on a sphere can be represented by a sum of spherical surface harmonics. We develop the space distribution of Equ. (1) into a series of spherical harmonics:

$$\Delta Q = \frac{a\,\ddot{Q}}{4\pi H r_0^2} f(t) \, g(z) \sum_n \sum_m Q_n^m P_n^m(\cdot) \cos m\tau \tag{4}$$

where $P_n^m(\cdot)$ are sphereical functions in Schmidt's normalization, $\cdot = \pi/2 - \rho$ is the co-latitude and

$$\tau = \Omega t + \lambda - \lambda_0$$

is the local time which is related to a "zero" longitude, $\cdot_0$ and is the midnight longitude during the onset of the geomagnetic storm, t = 0, while λ is the usual geographic longitude with respect to the Greenwhich merdian. ω is the angular frequency of the earth's rotation. Q is the total height and time integrated heat input (in erg) $\cdot r_0 \quad R_0 + z_0$, where R_0 is the earth's radius and z_0 is the lower boundary of the heat input.

Applying the well known properties of spherical functions (e. g., Chapman and Bartels, 1951), we derive from Equs. (4) and (1) the coefficients

$$Q_n^0 \quad (2n+1)\, P_n^0(\cdot_0) \left| \cos \frac{n\pi}{2} \right| \tag{5}$$

$$Q_n^m \quad \frac{2(2n+1)}{\pi m} P_n^m(\cdot_0) \sin \frac{m\pi}{2} \left| \sin \frac{n\pi}{2} \right| \quad (m > 0)$$

and

$$Q \quad F \frac{H}{a} \wedge Q_0 \tag{5a}$$

with

$$F \quad 2\pi r_0^2 \sin \cdot_0 \wedge \cdot_0$$

the total area where the heating occurs.

n, m	0, 0	2, 0	4, 0	6, 0	8, 0	1, 1	3, 1	5, 1	3, 3	5, 3
Q_n^m	1.00	3.66	2.22	-2.65	-6.91	0.807	3.58	5.26	-0.089	-0.589

Table 1: Spherical coefficient Q_n^m of the heat input. For details see text.

Table I contains the numberical values of Q_n^m of the lower domains (n, m) for a co-latitude of $\cdot_0 = 25°$ ($\varphi_0 = 65°$). We notice immediately that this series converges very slowly and that we need a large number of terms to approximate suffi-

ciently well our assumed heat input distribution of Equ. (1). This number is determined by the broadness of the disturbed region and is of the order of n 100 if the disturbed region has a thickness of about 500 km (5°). We shall see in the next section, however, that the thermosphere "filters out" the energy modes with large wave domain numbers n such that only the energy modes with low wave domain numbers become significant generators of the geomagnetic activity effect on the thermospheric density.

3. THE THERMOSPHERIC SYSTEM TRANSFER FUNCTION

In this section we want to determine the response of the thermospheric density to a heat input of the general form of Equ. (1). In order to do such calculations, we remember from system theory that the output response of a system, (t), can be calculated from the product of the system transfer function, G ( ), with the input frequency spectrum $\hat{Q}$ ( ):

$$(t) = \frac{1}{2\pi} \int_{-\infty}^{\infty} G(\omega)\, \hat{Q}(\omega)\, e^{j\omega t}\, d\omega \qquad (6)$$

where $\hat{Q}$ ( ) is the Fourier transform of the input Q (t) which is in our special case the heating function of Equ. (4) (e. g., Stein and Jones, 1967).

We can easily determine the frequency spectrum of the heat input of Equ. (4) which is in complex representation

$$\hat{Q}(\omega) = \frac{a\,\ddot{Q}}{4\pi r_0^2 H} \sum_n \sum_m \hat{Q}_n^m(\omega)\, P_n^m( )\, \exp\{j\, m\, (\lambda - \lambda_0)\} \qquad (7)$$

with

$$\hat{Q}_n^m(\omega) = \frac{Q_n^m\, g(z)}{a + j\,(\omega - m\,\Omega)}$$

It remains to determine the system transfer function G (·) of the thermospheric density. In order to do this, we again have to restrict ourselves to a highly idealistic model. For convenianee, we shall assume that perturbation theory is valid. Under this condition, full wave theory at thermospheric heights has shown that harmonic density waves behave like quasi-evanescent waves at altitudes above about 200 km. Their vertical dependence therefore can be approximated by

$$e^{-z/H_1} \tag{8}$$

where $H_1 > H_0$ is a real scale height which is slightly greater than the scale height of the quiet thermosphere H_0 (Volland, 1970). That means that these waves are attenuated very quickly outside of the location of thier generation and that one can neglect in a first approximation their propagation properties. Futhermore, we assume a time constant ion-neutral collision number ν_{col} of the order

$$\nu_{col} \approx 4 \times 10^{-4}\ sec^{-1} \tag{9}$$

at 350 km altitude. This collision number is much greater than the Coriolis term $2\Omega \cos$. Thus, we shall neglect the Coriolis force in the equations of horizontal momentum.

We set

$$\left.\begin{array}{c} \hat{p}_n^m \\ \hat{\rho}_n^m \\ \eta \dfrac{\partial \hat{u}_n^m}{\partial z} \sim \eta \dfrac{\partial v_n^m}{\partial z} \end{array}\right\} \propto e^{-z/H_1} \tag{10}$$

where $\hat{p}_n^m$, $\hat{\rho}_n^m$, $\hat{u}_n^m$ and $\hat{v}_n^m$ are the coefficients in a series of spherical harmonics of pressure, density and horizontal winds of the wave field in the frequency

domain. η is the coefficient of molecular viscosity. In that approach the vertical gradients of the horizontal winds tend to become zero with increasing height which is reasonable. Furthermore, we assume isothermal conditions for the quiet thermosphere with the mean values of pressure and density

$$\left.\begin{matrix} p_0 \\ \rho_0 \end{matrix}\right\} \propto e^{-z/H_0} \tag{11}$$

and set

$$\left.\begin{matrix} \hat{u}_n^m \\ \hat{v}_n^m \end{matrix}\right\} \propto \frac{\hat{p}_n^m}{p_0} \propto \exp\left\{-z\left(\frac{1}{H_1} - \frac{1}{H_0}\right)\right\}. \tag{12}$$

Then, from the equations of horizontal momentum conservation it follows for each term (n, m) of the wave in the frequency domain at the angular frequency ω:

$$\begin{aligned} (j\omega + \nu_{eff})\,\hat{u}_n^m\,Y_n^m + \frac{\hat{p}_n^m}{\rho_0\, r}\,\frac{\partial Y_n^m}{\partial \theta} &\sim 0 \\ (j\omega + \nu_{eff})\,\hat{v}_n^m\,Y_n^m \frac{\hat{p}_n^m}{\rho_0 \sin\theta}\,\frac{\partial Y_n^m}{\partial \lambda} &\sim 0 \end{aligned} \tag{13}$$

with

$$Y_n^m = e^{j\omega t}\,P_n^m(\theta)\,e^{jm(\lambda-\lambda_0)}$$

$$\nu_{eff} = \nu_{col} + \nu_{vis}$$

$$\nu_{vis} = \frac{\eta}{\rho_0\,\hat{u}_n^m\,H_1}\,\frac{\partial \hat{u}_n^m}{\partial z} \sim \frac{\eta}{\rho_0\,\hat{v}_n^m\,H_1}\,\frac{\partial \hat{v}_n^m}{\partial z}$$

$r = R_0 + z$ (R_0 = radius of the earth).

In our approximation, the viscosity force behaves like a collision term. It is of the order

$$\nu_{vis} \sim 1 \times 10^{-4}\ sec^{-1}$$

at 350 km altitude and remains constant with height. In a more exact treatment, it turns out that ν_{vis} slightly increases with height and becomes the dominant friction term above about 400 km (Geisler, 1967; Kohl and King, 1967).

Using Equ. (13), we determine the horizontal divergence of the wind field as

$$div\ \{(\vec{v}_n^m)\}_{hor} \sim \frac{n\,(n+1)\,\hat{p}_n^m\,Y_n^m}{r_0^2\,\rho_0\,(\nu_{eff} + j\,\omega)}. \tag{14}$$

Proceeding in a manner outlined in (Volland, 1970), we find from the equations of continuity and of the energy balance the following relationship between the frequency domains of heat input and density:

$$\frac{\hat{\rho}_n^m}{\hat{Q}_n^m} \cdot G_n(\omega) = \frac{1}{1/R_i + j\,\omega\,C + \dfrac{1}{R_n + j\,\omega\,L_n}} \tag{15}$$

with

$$C = \frac{2\,(\alpha - 1)\,c^2}{(\gamma - 1)} \sim 4 \times 10^9\ [cm^2/sec^2]$$

$$R_i = \frac{H_1\,\hat{\rho}_n^m}{2\,\kappa\,\partial\,\hat{T}_n^m/\partial\,z} \sim 1 \times 10^{-5}\ [sec^3/cm^2]$$

$$R_n = -\frac{\gamma^2\,r_0^2\,\nu_{eff}}{\omega^2\,c^4\,n\,(n+1)} \sim \frac{4 \times 10^{-4}}{n\,(n+1)}\ [sec^3/cm^2]$$

$$L_n = \frac{\gamma^2 r_0^2}{2 \alpha^2 c^4 n (n+1)} \sim \frac{8 \times 10^{-3}}{n (n+1)} \ [sec^4/cm^2]$$

$\alpha = H_1/H_0 \sim 1.15$

$\gamma = 1.5$ (ratio between the specific heats)

$c = 840$ m/sec (velocity of sound)

$\kappa =$ (coefficients of the heat conduction).

The numbers of R_i and α have been adopted from full wave calculations done for the domain numbers (0, 0), (2, 0) and (1, 1) at a frequency of $\omega = \Omega$ for a thermospheric model of exospheric temperature of $T_\infty = 1000°K$ and assuming $H = H_0$. They are valid within the height range between 300 and 400 km. These numbers will be kept constant, independent on n or α in our approach, though this is certainly a rough approximation. As we shall see in the following, the wave coefficients of the three above mentioned wave domain numbers play the predominant role for the geomagnetic activity effect. Therefore, we expect that our approximation gives rise to errors which are not too serious.

The physical meaning of the different terms in Equ. (15) is the following:

Equ. (15) which is essentially the first law of thermodynamics contains two reversible terms which describe the adiabatic increase of internal energy of the gas (the term C) and the work done by the gas (the term L_n), the last one mainly due to horizontal winds. The dissipative terms are due to vertical heat conduction (the term R_i) and due to horizontal ion drag and viscosity (the term R_n). Both terms behave like heat sinks which take energy out of the wave and

convert it into internal energy of the surrounding gas. It is apparent from Equ. (15) that at very low frequencies only the dissipative terms are effective. In the case of the zero component (n = 0) wave dissipation is solely due to vertical heat conduction. For the higher wave domain numbers (n > 0) horizontal ion drag and viscosity become increasingly important as dissipation mechanism because the horizontal scale length of the wave structure decreases with increasing n.

The system transfer function $G_n(\omega)$ of Equ. (15) which only depends on the wave domain number n has the form of the amplification factor of an R-amplifier with L-equalizer (the block diagram of which is shown in Fig. 1):

$$G_n(\omega) = \frac{u_a}{u_g} \tag{16}$$

Here, $u_g \triangleq \hat{Q}_n^m R_i$ is the grid voltage of a triode, R_i is the internal resistance of the triode, $u_a \triangleq \hat{\rho}_n^m$ is the anode voltage and R_n, L_n and C are resistor, inductor and capacitor of the anode circuit. The properties of such an amplifer are described in every textbook of system theory.

In Fig. 2 we plotted the magnitude of G_n versus frequency ω with the wave domain number n as parameter. We notice that for small numbers n the transfer G_n behaves like a low pass filter with bandwidth of

$$\Omega_0 \sim R_n/2\,L_n = \nu_{eff}/2 \sim 2.5 \times 10^{-4}\ \mathrm{sec}^{-1}. \tag{17}$$

The anode resistor R_n and the inductor L_n decrease with n. Thus, the anode circuit becomes a short circuit with increasing n, and the amplification decrease like $1/n^2$ for $n >> 1$. However, in the vicinity of

$$C = \frac{L_n}{R_n^2 + \omega^2 L_n^2} \quad \text{or} \quad \omega = \Omega_n \sqrt{\frac{1}{C L_n} - \nu_{eff}^2} \tag{18}$$

there occurs a resonance peak due to the over equalizing effect of the inductor L_n. It gives rise to a maximum of G_n of

$$|G_n|_{max} = \frac{1}{1 R_i + \nu_{eff} C} \quad \text{for} \quad n >> 1 \tag{19}$$

which is independent of n.

That resonance effect can already be seen from a simple theory of plane internal gravity waves. In order to compare our result with plane wave theory, we notice that the zonal spherical functions P_n^0 have n zeros between $0 \leq \theta \leq 180°$. Thus, their "horizontal wave length" is

$$(\lambda_x)_n \sim \frac{2 \pi r}{n} \quad (n >> 1)$$

and their normalized "horizontal wave number" for the resonance frequencies Ω_u is

$$S = \frac{c}{\Omega_n} (k_x)_n \sim \frac{n c}{r_0} \sqrt{C L_n} \sim \sqrt{\frac{(\alpha - 1)}{(\gamma - 1)}} \frac{\gamma}{\alpha} \sim 1 \quad (n >> 1). \tag{20}$$

The range $1 \lesssim S < 2$ is just the range where the attenuation of plane internal gravity waves has it minimum (e. g., Volland, 1969b). However, its deepness is much smaller at altitudes above about 300 km than Fig. 2 suggests and in fact nearly disappears at 400 km altitude. Therefore, we must conclude that our approach, though being qualitatively consistent with the exact theory, overestimates the amplification effect of the thermospheric circuit for great wave domain

numbers n. The reason for that discrepancy lies in our assumption of constant circuit elements R_i and n (n + 1) R_n, on the one hand. One the other hand, viscosity and heat conduction due to horizontal gradients of winds and temperature which are neglected in our approach lead to an additional decrease of G_n for great domain numbers n. Our whole concept of course breaks down for accoustic wave ($\omega > 10^{-2}$ sec^{-1}).

The resonance frequencies Ω_n lie well beyond the collision frequency ν_{eff}. Therefore, the error due to our approach involves predominantly the high frequency band of the disturbance. As we shall see in the next section, the decay factor a in Equ. (3) related to an average geomagnetic disturbance is of the order

$$a \sim \Omega << \Omega_n, \quad (n > 3),$$

and the bandwidth of the spectral function $\hat{Q}_n^m$ in Equ. (8) is therefore

$$\Omega_0 \sim \Omega.$$

Thus, the low frequency tail of the disturbances which contains most of the spectral energy is not affected very much by the high frequency range G_n.
Because of these reasons, is appropriate to make a further simplification by taking the inductor $L_n = 0$. That gives the simplified system transfer function

$$\overline{G}_n(\omega) = \frac{1}{1/\overline{R}_n + j\omega C} \tag{21}$$

with

$$\frac{1}{\overline{R}_n} = \frac{1}{R_i} + \frac{1}{R_n}.$$

Now, $\bar{G}_n(\omega)$ resembles the reziprocal impedance of a simple RC-circuit.

The magnitudes of $\bar{G}_n$ are plotted as dashed lines in Fig. 2 and indicate that only the high frequency band of G_n for great n is changed by that simplification.

4. THE DENSITY RESPONSE AS FUNCTION OF TIME

In this section we want to determine the density disturbance in the time domain caused by the heat input of Equ. (4) and by the system transfer function $\bar{G}(\omega)$ given by Equ. (21). As already mentioned, by using $\bar{G}(\omega)$ instead of $G(\omega)$ of Equ. (15) we suppress the high frequency response of the density disturbance and consider only the slow tail of the disturbance. The transformation from the frequency domain into the time domain using Equ. (6) leads to a density distrubance of

$$\Delta\rho = \frac{a\,\bar{Q}}{4\,\pi\,r_0^2\,H}\,g(z)\sum_n\sum_m \rho_n^m(\lambda,\,t)\,P_n^m(\vartheta) \tag{22}$$

with

$$\rho_n^m(\lambda,\,t) = \frac{Q_n^m}{A_n^m\,C}\left\{e^{-at}\cos(m\,\tau - \alpha_n^m) - e^{-b_n t}\cos(m(\lambda-\lambda_0) - \alpha_n^m)\right\}$$

and

$$A_n^m = \sqrt{(b_n - a)^2 + m^2\,\Omega^2}$$

$$\alpha_n^m = \tan^{-1}\left\{\frac{m\,\Omega}{(b_n - a)}\right\}$$

$$b_n = \frac{1}{C\,\bar{R}_n} = \frac{1}{C}\left(\frac{1}{R_i} + \frac{1}{R_n}\right)$$

Since A_n^m increases with n and m, the coefficients with large domain numbers (n, m) are filtered out rather rapidly within the thermospheric "circuit system". The density distribution of Equ. (22) not only depends on the storm time t but also on local time τ. We shall discuss first that part of the density disturbance which only depends on storm time (m = 0).

4.1 The Zonal Components

For the zonal components (m = 0) it is

$$\rho_n^0 = \frac{Q_n^m}{C} \frac{\{e^{-at} - e^{-b_n t}\}}{(b_n - a)} \tag{23}$$

That coefficient has a maximum value of

$$(\rho_n^0)_{max} = \frac{Q_n^m}{C\, b_n} e^{-a(t_{max})_n^0}$$

at the time

$$(t_{max})_n^0 = \frac{1}{b_n} \frac{1}{(x_n - 1)} \ln x_n \tag{24}$$

with

$$x_n = \frac{a}{b_n} .$$

That, time of the maximum shifts toward lower values as x_n increases. From the numerical values in Equ. (15) it follows

$$b_0 = 1/(R_i\, C) \sim 2.5 \times 10^{-5}\ sec^{-1}.$$

From the observed averaged time lag between geomagnetic disturbances and the thermospheric geomagnetic activity effect of $(t_{max})_0^0 \sim 5.5$ hours we determine

$$b_0 (t_{max})_0^0 \sim 0.5$$

and from Eq. (24)

$$a \sim 10^{-4} \text{ sec}^{-1}. \tag{25}$$

The time of maximum of the ρ_2^0-coefficient then becomes

$$(t_{max})_2^0 \sim 4300 \text{ sec}^{-1} \sim 1.1 \text{ hours},$$

and it is

$$(t_{max})_n^0 < (t_{max})_{n-1}^0.$$

Thus, the wave components with wave numbers $n > 2$ are significant only within the first hour after the commencement of the disturbance and then decay rapidly.

In Fig. 3a we plotted the coefficients ρ_n^0 (t) of the density versus storm time t for the wave domain numbers 0, 2, 4, 6, and 8 using the values of Q_n^0 from Table 1. and the number, a, from Equ. (25)*. We note that in spite of the larger coefficients Q_n^0 as compared with $Q_0^0 = 1$, the zero coefficient ρ_0^0 (t) dominates about 3 hours after the beginning of the disturbance.

The two first coefficients ρ_0^0 and ρ_2^0 already dominate 30 minutes after the beginning of the disturbance. However, the higher harmonics with $n > 2$ may produce significant amplitudes within the first 30 minutes. Therefore, we expect an oscillating behavior at the beginning of the disturbance which can not be produced in our simlified theory.

* Positive values are indicated by solid lines, negative values are indicated by dashed lines.

The sum of the zonal components is plotted versus storm time t in Fig. 3b for four different latitudes $\varphi = 0°$, 30°, 60° and 90°. Here we note a shift of the maximum disturbance in the density from 6 h at the equator ($\varphi = 0°$) to 2.5 h at the poles ($\varphi = \pm 90°$) and an increase of the maximum density amplitude by a factor of about two between equator and poles. Fig. 4 presents that latitudinal dependence of the zonal maximum amplitudes and the zonal maximum times versus latitude. That latitudinal behavior is essentially due to the influence of the zonal harmonic P_2^0 which is positive at latitudes $|\varphi| > 35°$ and negative at lower latitudes.

The total duration of the impulse is of the order of two days. At the equator the initial phase is negative during the first hour. Ten hours after the start of the disturbance the amplitudes of the zonal components with $n > 0$ are decayed and there remains only the zero components $\rho_0^0 P_0^0$.

In order to study the influence of the shape of the heat input on the density disturbance we varied the decay factor a of the heat input and calculated the corresponding times of maximum $(t_{max})_0^0$ and the maximum amplitudes $(\rho_0^0)_{max}$ of the zero component. We plotted a and $(\rho_0^0)_{max}$ versus $(t_{max})_0^0$ in Fig. 5a. Moreover, we determined in Fig. 5b the total duration ΔT of the impulse versus maximum time. That total duration is not uniquely defined because of the exponential decay of the density disturbance. Therefore, we define that the end of the disturbance is reached where the amplitude has dropped to

$$\rho_0^0 (t = \Delta T) = 3 \times 10^{-8} \text{ sec}^3/\text{cm}^2$$

In our example in Fig. 3b that condition is equivalent to a ratio

$$\rho_0^0 (t = \Delta T)/(\rho_0^0)_{max} \sim 10^{-2}$$

That ratio becomes greater with decreasing a-factor and vice versa (see Fig. 5a) and shall take account of the fact that in practical data processing the evaluation of a disturbance is limited by an absolute noise level rather than by a relative amplitude ratio. Fig. 5s shows that the total duration ΔT increases with increasing time maximum $(t_{max})_0^0$. If we use any other definition for the duration of the disturbance we change the slop of the curve in Fig. 5b without changing the trend.

The results of Fig. 4 and 5 should be compared with available satellite drag data. The decrease of the time of maximum with increasing latitude is in agreement with the analysis of Jacchia et al., (1967) and Roemer (1967). The increase of the maximum amplitude by a factor of about two between equator and poles agrees with Roemers (1970) analysis. However, in Roemers (1970) paper, he did not confirm the latitudinal dependence of the mean values of the maximum time but claims that there is no significant dependence*. We shall return to that discrepancy between observation and theory in section 4.2. Roemer (1970) also determined a relationship between duration of the impulse and the time of maximum and found a linear dependence (the dash-dotted line in Fig. 5b). That observation is sufficiently well reproduced by our theroy.

Fig. 5a also shows a relation between the decay factor a and the maximum amplitude $(\rho_0^0)_{max}$. That maximum decreases rapidly with increasing, a, indicating that isolated short periodic polar substorms lasting typically one hour ($a \sim 10^{-3}$ sec^{-1}) do not generate a significant geomagnetic activity effect.

* Though his individual data scatter widely from 0 to 15 hours within the whole range of latitude.

We can estimate the amount of heat input necessary to cause the observed density disturbance during magnetic storms. From Roemers (1970) analysis, we determine an increase of the exospheric temperature of $\Delta T_c = 50°$ K at a latitude of $\varphi = 0°$ for a geomagnetic index of $K_p = 3$. That increase of the exospheric termperature in turn is related to a maximum relative density amplitude of

$$\Delta\rho_{max}/\rho_0 \quad 0.17 \tag{27}$$

or

$$\Delta\rho_{max} \quad 1.4 \times 10^{-15} \text{ g/cm}^3$$

at moderate solar activity and at 350 km altitude. The total heat input integrated over time and space is then according to Equ. (22)

$$\bar{Q} \quad \frac{4\pi r_0^2 H \Delta\rho_{max}}{g(z)\, a \left\{\sum_n {}^0_n P^0_n\right\}_{max}} \quad 2 \times 10^{22} \text{ erg} \tag{28}$$

where $r_0 = 6500$ km, $z = 350$ km and $H \quad H_0 = 50$. From the solid curve with parameter $\varphi = 0°$ in Fig. 4, a maximum value of

$$\left\{\sum_n {}^0_n P^0_n\right\}_{max} \quad 1.4 \times 10^{-6} \text{ sec}^3/\text{cm}^2$$

was used.

The total heat input of Equ. (28) should be compared with an estimate made by Akasofu (1968) for the energy content carried by the auroral electrons and the ring current protons during a polar substorm. His estimate is 2×10^{22} erg.

Comparing this number with our value in Equ. (28) we have to conclude that a moderate geomagnetic storm should contain at least three times the energy of a substorm if we assume an efficiency factor for the heat transfer of $\cdot \leq 0.3$.

Within the auroral belts the maximum height integrated heat input is according to Eq. (5a)

$$H \Delta Q_0 = \bar{Q} \frac{a}{F} \sim 20 \text{ erg}/(\text{cm}^2 \text{ sec})$$

where the numbers $F = 1 \times 10^{17}$ cm^2; $\theta_0 = 25°$ and $\Delta \theta_0 = 5°$ have been adopted. That value seems to be not unrealistically large. The maximum heat input at $t = 0$ within a vertical column averaged over the whole sphere is

$$a Q/(4 \pi r_0^2) \sim 0.4 \text{ erg}/(\text{cm}^2 \text{ sec}).$$

That value is only a fraction of the XUV-input into the thermosphere above 100 km (Hinteregger et al., 1965).

4.2 The Local Time Dependence of the Density Disturbance

We now turn to the discussion of that part of the density disturbance in Equ. (22) which depends on local time τ. This part is connected with the associated spherical functions P_n^m $(m > 0)$. In Fig. 6 we plotted the coefficients p_n^m $(m > 0)$ versus storm time from Equ. (22) adopting the number a from Equ. (25) and the coefficients Q_n^m from Tab. I. Fig. 6a is calculated for the longitude of $\lambda - \lambda_0 = 0°$, and Fig 6a is valid for a longitude $\lambda - \lambda_0 = 90°$. The curves for the longitude of 180° and of 270° differ from those of Fig. 6a and 6b, respectively, by only a change in sign. Positive values in Fig. 6 are indicated by solid lines, negative values by dashed lines. From Fig. 6 we note that the coefficients with larger

wave numbers n peak earlier than those with lower wave numbers, a fact which we observed have from the behavior of zonal coefficients in Fig. 3. Moreover, the coefficients with m = 3 are of no signifiance throughout the temporal range considered. This again is due to the small excitation factors of waves with large wave domain numbers (n, m). Two hours after the onset of the distrubance the predominant coefficient remains ρ_1^1. During its maximum phase that coefficient is positive at local night and negative at local noon. Thus it contributes to the total density disturbance in such a manner that it increases the effect during the night and decreases it during the day. This behavior becomes more clear in Fig. 7 where we plotted the total density disturbance $\sum_{n,m} \rho_n^m P_n^m$ versus storm time for the three latitudes $\varphi = 0°$, $30°$ and $60°$ and for four different longitudes $\lambda - \lambda_0 = 0°$, $90°$, $180°$ and $270°$. In Fig. 7 we omitted the curves valid at the poles ($\varphi = 90°$) because they are identical with the corresponding curve in Fig. 3b and show no dependence on local time.

As is already obvious from Eq. (22), the shape of the disturbance, its maximum amplitude and maximum time depend on storm time, local time and individual longitude of each event.

The maximum amplitudes and the times of maximum for the total density disturbance are plotted versus longitude in Fig. 8a and 8b for the four latitudes considered. The maximum amplitude shows a quasi-harmonic variation with longitude with maximum values about $\lambda - \lambda_0 = 330°$. The amplitudes of the curves in Fig. 8a are largest at $60°$ latitude, the amplitudes of the maximum times in Fig. 8b are largest at the equator. If we had plotted these curves versus local time we had to shift the abszissa in Fig. 8 by Ωt_{max}. Then, the maximum of the curves in Fig. 8a occurs at about

$\lambda_{t_{max}} + 330° \sim 0°$ to 90° (0h to 6h Lt)

that is during the early morning hours, if we consider the range of the times of maximum from Fig. 8b to be 2h to 8h Lt.

We compare the result of Fig. 8 with observations of Roemer (1970). Roemer found a dependence of the maximum amplitudes on local time at low latitudes which is consistent in magnitude and phase with our result of Fig. 8a. However, he did not observe a signicant longitudinal dependence of the maximum times as we predict in Fig. 8b. A possible explanation for that discrepancy as well as for the similar discrepancy concerning the latitudinal dependence of the maximum times (see section 4.1) may be the fact that each individual geomagnetic activity effect depends on its own midnight longitude λ_0. Observations at longitudes arbitrarily related to that λ_0 lead to a wide scattering of data for the maximum times between 1.4 and 8 hours in our special case of Fig. 8b. Moreover, these data depend on the decay factor, a, of every individual storm. Finally, the problem becomes even more complicated by the facts that (a), the temporal behavior of any individual storm may be far from similar to our assumed simple exponential model of Eq. (3) and (b), that with increasing intensity of the storm the auroral ovals shift to lower latitudes, thus influencing the ratios between the spherical coefficients of the heating function in Eq. (4). At present, therefore, these discrepancies remain open questions. We would suggest that geomagnetic activity should be studied in terms of the midnight longitude λ_0 of each individual storm.

5. DISCUSSION AND CONCLUSION

In the foregoing sections we considered on impulse type heat input within a small band of latitude near the auroral ovals during local night. We determined the

"system transfer function" of the thermospheric density and calculated from that function and from the Fourier spectrum of the heat input the temporal response of the thermospheric density to the heat input. It appears that the components with large wave domain numbers (n, m) have excitation factors which decrease rapidly with increasing numbers (n, m). Thus, after the onset of the geomagnetic storm, the density distribution of the geomagnetic activity effect can be described by the four spherical harmonics with the lowest wave domain numbers. Three hours after the onset of the disturbance the zero component (0, 0) dominates and leads to a slow tail of the density amplitude and thus to the observed global response of the thermospheric density. We examined its dependence of this effect on storm time, latitude and longitude and compared the theory with available satellite drag data. While the dependence of the maximum amplitude on latitude and longitude could be well reproduced in this theory, a discrepancy remains between observations by Roemer (1970) and our calculations. This concerns the dependence on latitude and longitude of the times of maximum for geomagnetic activity effect which is not significant according to Roemer. We suggest that this discrepancy may be due to the dependence of the geomagnetic activity effect on storm time which has not been taken into account in an appropriate manner in previous treatments.

Our theory does not appropriately describe the high frequency range of the geomagnetic activity effect which might be significant during the first hour of the disturbance, Thus we have excluded short periodic gravity waves and accoustic waves which have in fact been observed in the vicinty of the auroral zones just after the beginning of the geomagnetic disturbance (Taeusch and Carignan, 1970; Tastud, 1970). These disturbances can not be detected from satellite drag data due to the poor time resolution of this method which is not better than

three hours. Also, the short periodic geomagnetic bay disturbances or polar substorms do not supply enough spectral energy into the slow tail to become detectable by the satellite drag method. These short period disturbances may be described more appropriately in terms of plane gravity wave propagation (e. g. Chimonas and Hines, 1970).

Our theory is appropriate essentially for the explanation of the satellite drag data which observe the slow tail of the geomagnetic activity effect. The slow tail however contains most of the spectral energy of an event with a typical duration of one day.

The local time dependent component (1, 1) of that slow tail gives rise to horizontal winds which are similar in structure to the winds of the tidal (1, -1) mode at lower altitudes which are however shifted in phase by about 120° with respect to the tidal wind. In the light of that result one should reconsider the orgin of the geomagnetic SD-current in terms of dynamo theory. As Fukushima and Oguti (1953) showed, dynamo theory can explain the SD-current if the wind is shifted in phase by 100° to 150° with respect to the wind responsible for the Sq-current. Since the wind of the Sq-current is the wind of the tidal (1, -1) mode (Stening, 1969) and since the phase of the wind of the geomagnetic activity effect is shifted in the right manner, we suggest that at least part of the geomagnetic SD-current may be generated within the thermosphere by the dynamo action of winds related to the geomagnetic disturbance.

6. LITERATURE

Akasofu, S., Polar and magnetospheric substorms, Reidel Publ. Comp., Dortrecht 1968

Chapman, S. and J. Bartels, Geomagnetism, The Claredon Press, 1951

Chimonas, G. and C. O. Hines, Atmospheric gravity waves launched by auroral currents, Planet. Space Sci. 18, 1970, 565-582

Cole K. D., Electrodynamic Heatup and Movement of the Thermosphere, to be published in Planet. Space Sci., 1970

Fukushima, N. and T. Oguti, Polar magnetic storms and geomagnetic bays, Rep. Ionosphere Space Res. Japan, 7, 1953, 137-146

Geisler, J. E., A numerical study of the wind system in the middle thermospheric, Journ. Atm. Terr. Phys. 29, 1967, 1469-1482

Hinteregger, H. E., Hall, L. A. and G. Schmidtke, Solar XUV radiation and neutral particle distribution by July 1963 thermosphere, Space Res. V, p. 1175-1190, North-Holland Publ. Comp., Amsterdam 1965

Jacchia, L. G., Two atmospheric effects in the orbital acceleration of artifical satellite, Nature, 183, 1959, 526-527

Jacchia, L. G. and J. Slowey, An analysis of the atmospheric drag of the Explorer IX satellite from precisely reduced photographic observations Space Res. IV, p. 257-270, North-Holland Publ. Comp., Amsterdam 1964a

Jacchia, L. G. and J. Slowey, Atmospheric heating in the aurora zones: a preliminary analysis of the atmospheric drag of the Injun 3 satellite, Journ. Geophys. Res. 69, 1964b, 905-910

Jacchia, L. G., Slowey, J. and F. Veriani, Geomagnetic perturbations and upper atmospheric heating, Journ. Geophys, Res. 72, 1967, 1423-1434

Kohl, H. and J. W. King, Atmospheric winds between 100 and 700 km and their effects on the ionosphere, Journ. Atm. Terr. Phys, 29, 1967, 1045-1062

Roemer, M. Geomagnetic activity effect derived from Explorer IX data, Phil. Trans. Roy. Soc. A262, 1967, 185-194

Roemer, M., Geomagnetic activity effect in the 250 to 800 km altitude region, Space Res. XI, 1970

Stein, S. and J. J. Jones, Modern communication principles, McGraw Hill Comp., New York, 1967

Stening, R. J., An assessment on the contribution of various tidal winds to the Sq current system, Planet. Space Sci. 17, 1969, 889-908

Taeusch, D. R. and G. R. Carignan, Neutral composition variation in the aurora zone during a magnetic storm, AGU Fall meeting, San Francisco, 1970

Testud, J., Gravity waves generated during magnetic substorms, Journ. Atm. Ter. Phys. 32, 1970, 1793-1805

Thomas, G. E. and B. K. Ching, Upper atmospheric response to transient heating, Journ. Geophys. Res. 74, 1969, 1796-1811

Volland, H., A theory of thermospheric dynamics-II, Planet. Space Sci. 17, 1969a, 1709-1724

Volland, H., The upper atmosphere as a multiply refractive medium for neutral air motions, Journ. Atm. Terr. Phys. 31, 1969b, 491-514

H. Volland, The thermospheric density variations as an oscillator circuit system, Ann. Geophys. 26, 1970, 523-530

FIGURE CAPTION

Fig. 1 Block diagram of an R-amplifier with L-equalizer

Fig. 2 Magnitude $|G_n|$ of the "signal transfer function" of the thermospheric density versus angular frequency ω. The wave domain number n is shown for each curve. The dashed curves give the approximate function $|\bar{G}_n|$. For details see text.

Fig. 3a Zonal coefficients ρ_n^0 versus storm time t. Full lines indicate positive values, dashed lines indicated negative values.

Fig. 3b Sum of zonal components $\Sigma \rho_n^0 P_n^0$ versus storm time t for four different latitudes φ.

Fig. 4 Maximum amplitudes (solid lines) and times of maximum (dashed lines) of the sum of the zonal components (Fig 3b) versus latitudes φ.

Fig. 5a Maximum amplitude $(\rho_0^0)_{max}$ and decay factor a of the heat input versus maximum time $(t_{max})_0^0$ of the zero component.

Fig. 5b Total duration ΔT of the density disturbance versus time of maximum $(t_{max})_0^0$ of the zero component.

Fig. 6 Spherical components $\rho_n^m P_n^m$ $(m > 0)$ versus storm time t calculated at the equator $(\varphi = 0°)$. Solid lines indicate positive values, dashed lines indicate negative values.

a) Longitude $\lambda - \lambda_0 = 0°$

b) Longitude $\lambda - \lambda_0 = 90°$

Fig. 7 Sum of all components $\sum_{n,m} \mu_n^m P_n^m$ versus storm time t for three different latitudes φ and four different longitudes $\lambda - \lambda_0$.

Fig. 8 Maximum amplitudes (Fig. 8a) and maximum times (Fig 8b) taken from Fig. 7 versus longitude $\lambda - \lambda_0$ for four different latitudes φ.

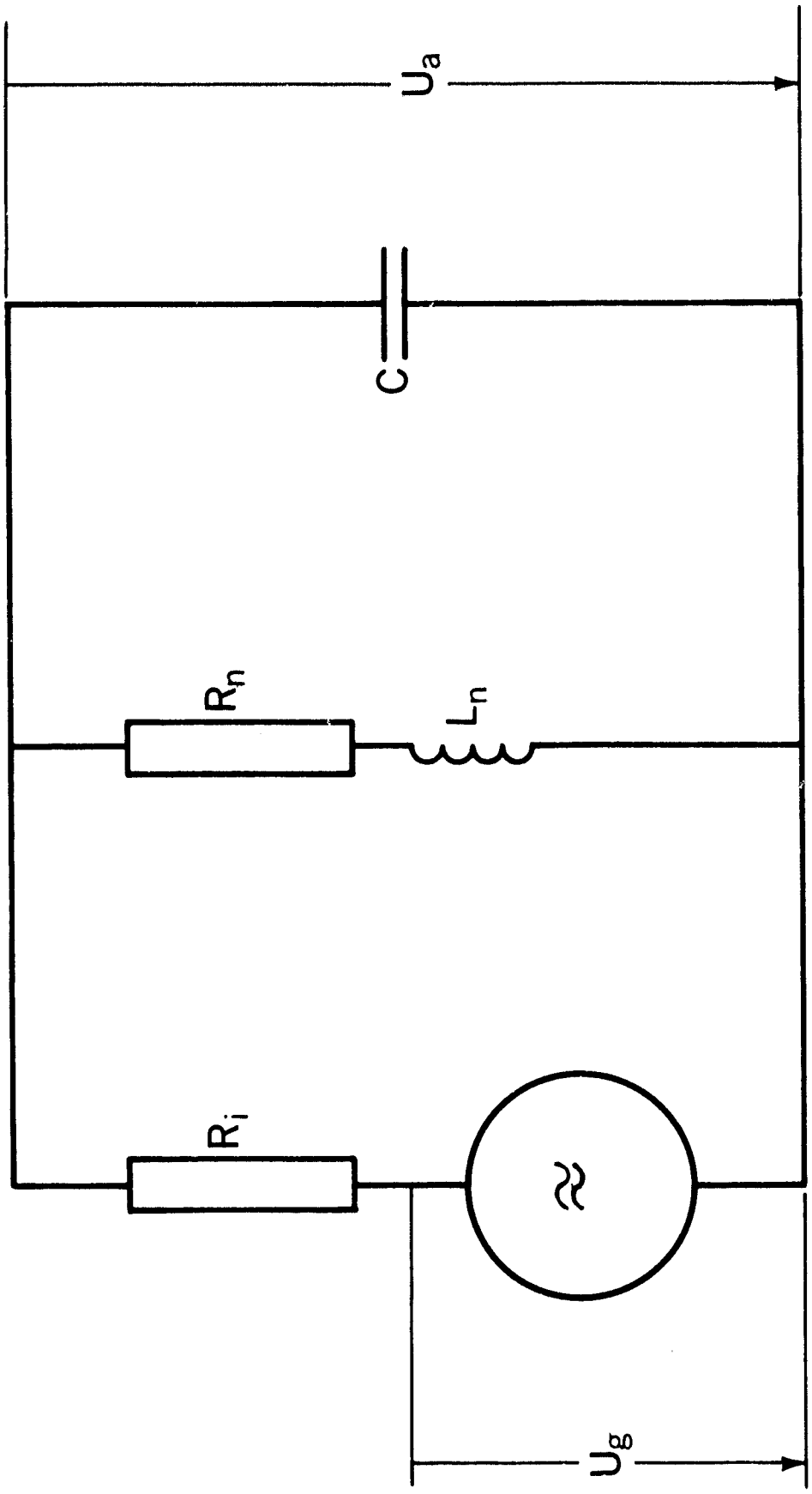

Figure 1. Block diagram of an R-amplifier with L-equalizer

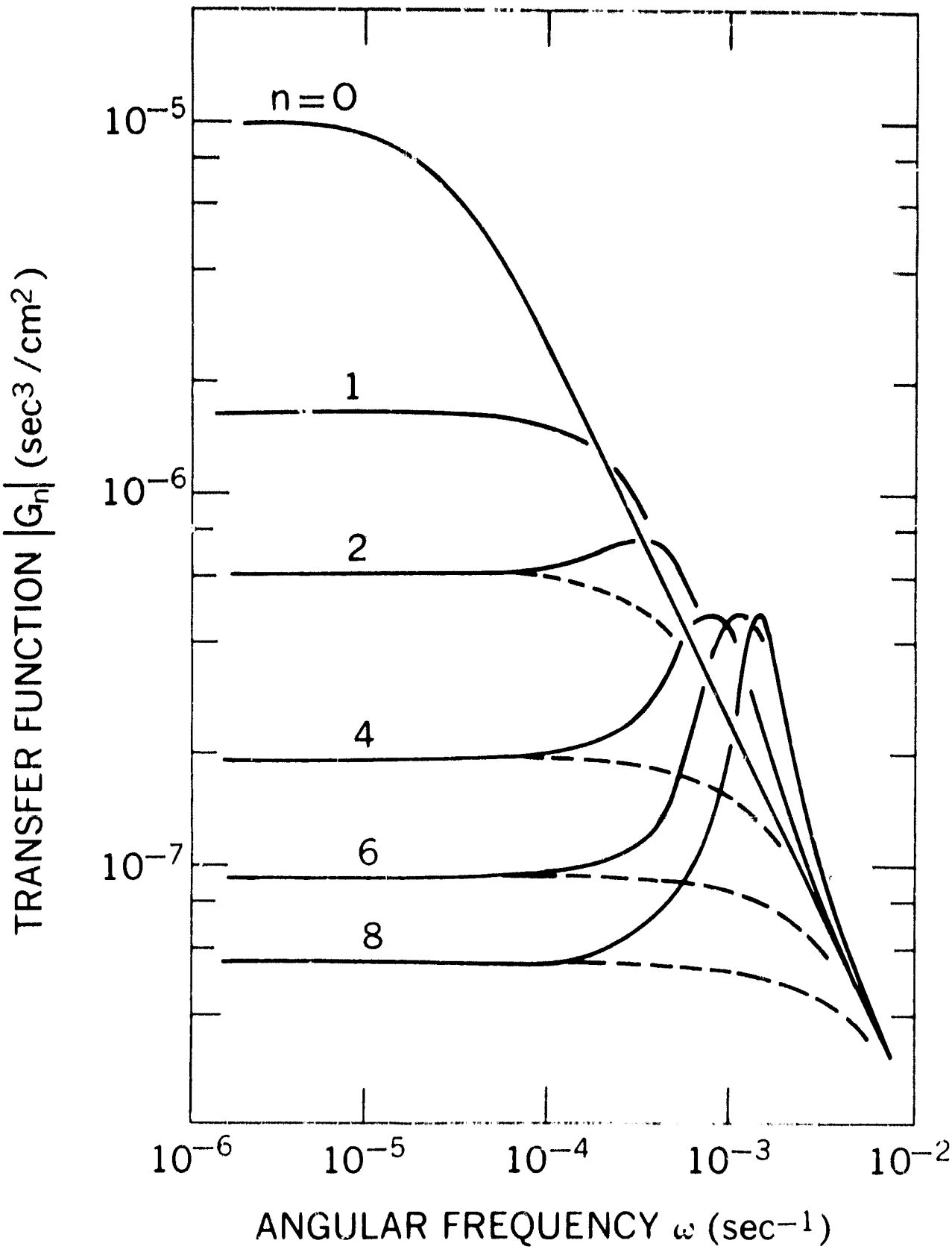

Figure 2. Magnitude $|G_n|$ of the "signal transfer function" of the thermospheric density versus angular frequency ω. The wave domain number n is shown for each curve. The dashed curves give the approximate functions $|G_n|$. For details see text.

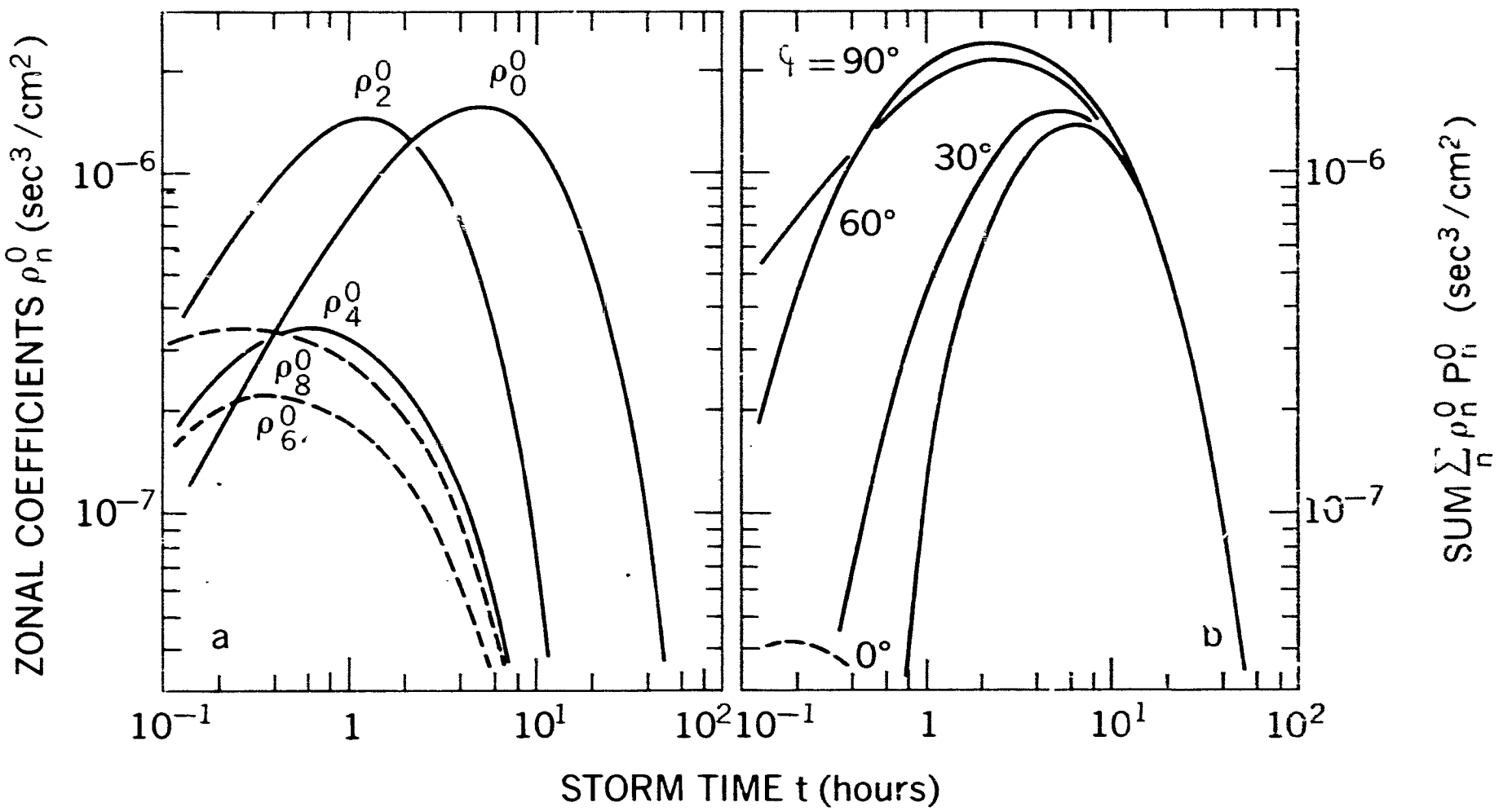

Figure 3a. Zonal coefficients ρ_n^0 versus storm time t. Full lines indicate positive values, dashed line indicate negative values.

Figure 3b. Sum of zonal components $\sum_n \rho_n^0 P_n^0$ versus storm time t for four different latitudes φ

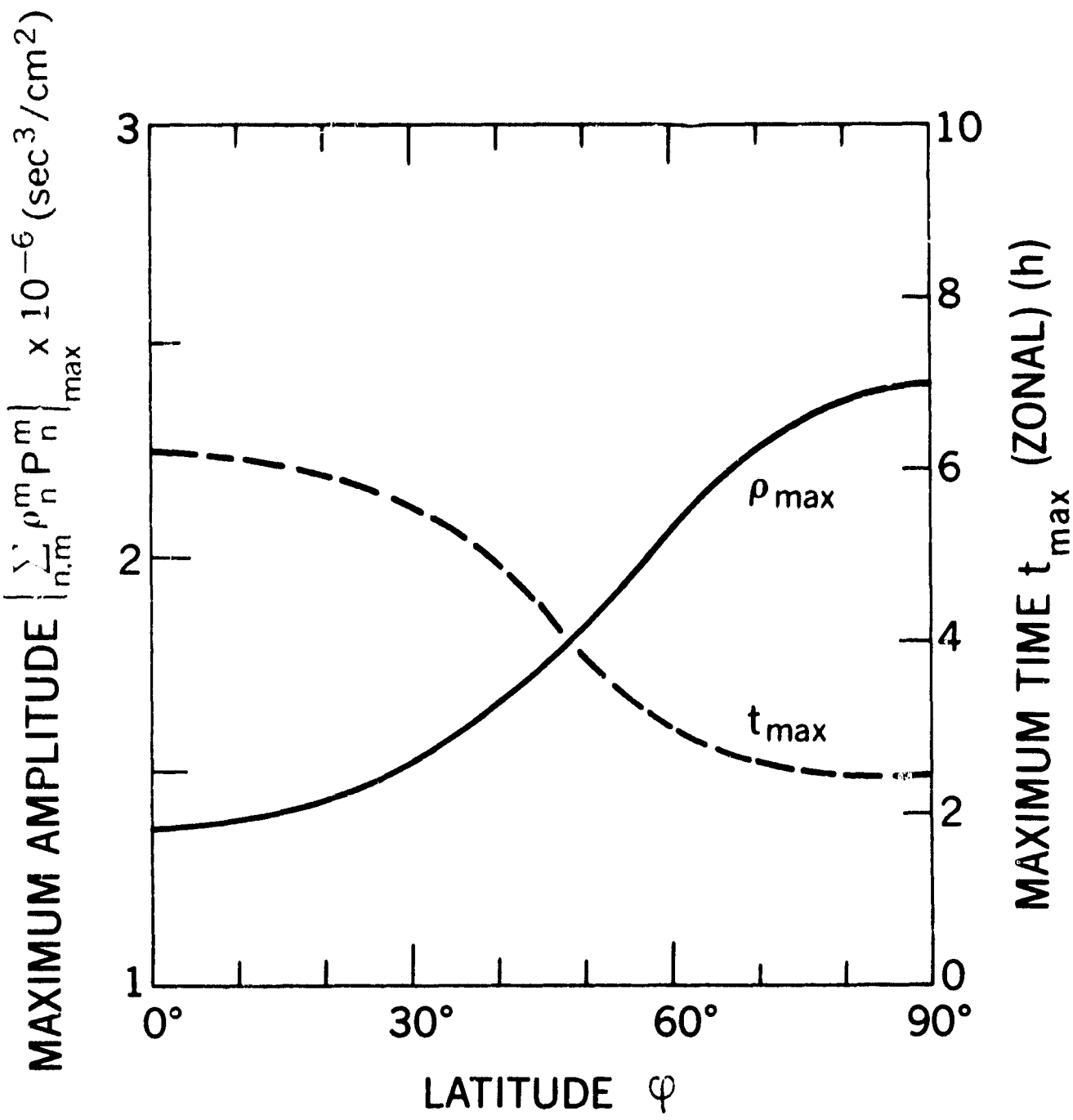

Figure 4. Maximum amplitudes (solid lines) and maximum times of (dashed lines) of the sum of the zonal components (Figure 3b) versus latitude φ

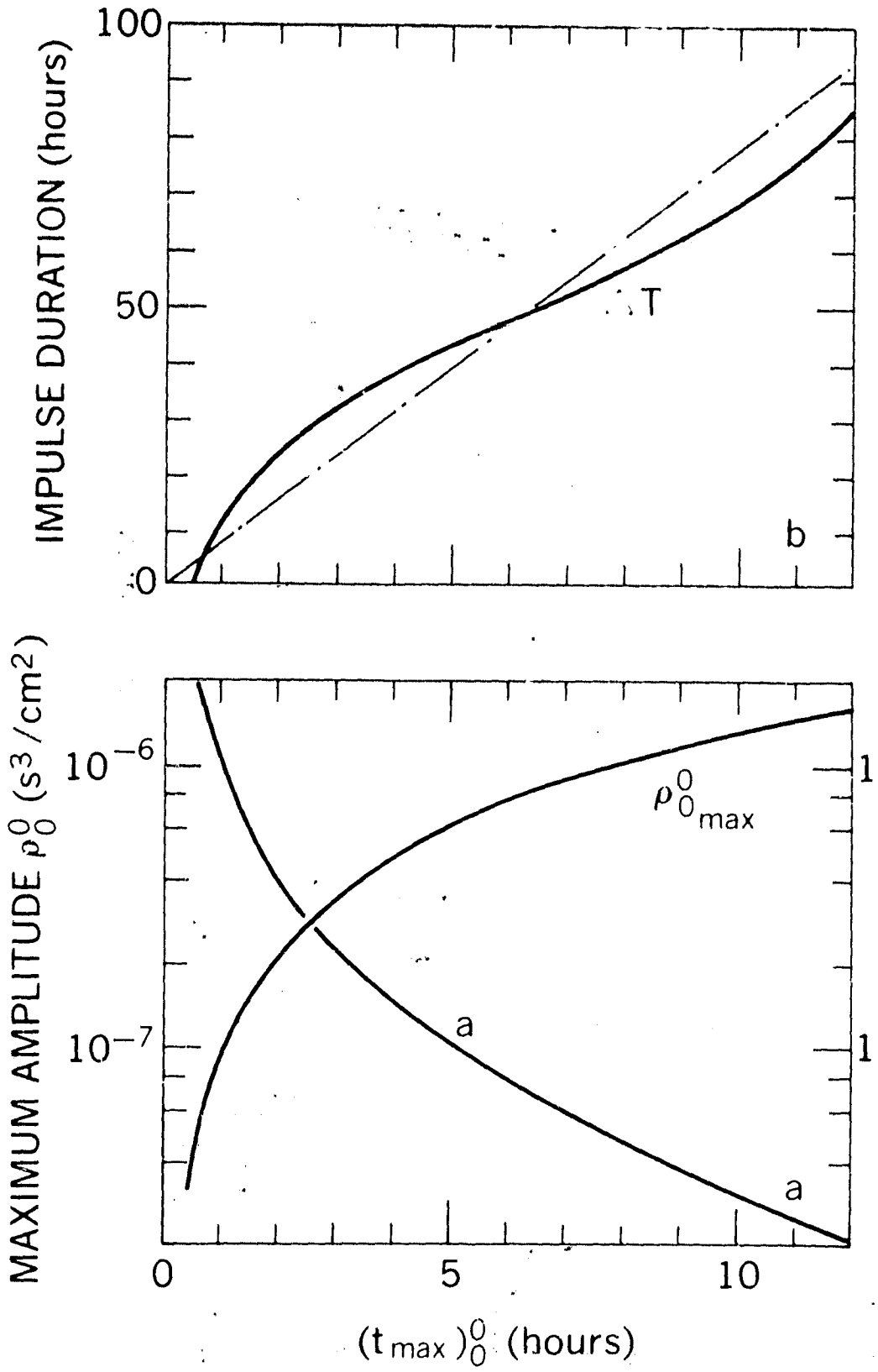

Figure 5a. Maximum amplitude $(\rho_0^0)_{max}$ and decay factor a of the heat input versus maximum time $(t_{max})_0^0$ of the zero component.

Figure 5b. Total duration ΔT of the density disturbance versus maximum time $(t_{max})_0^0$ of the zero component.

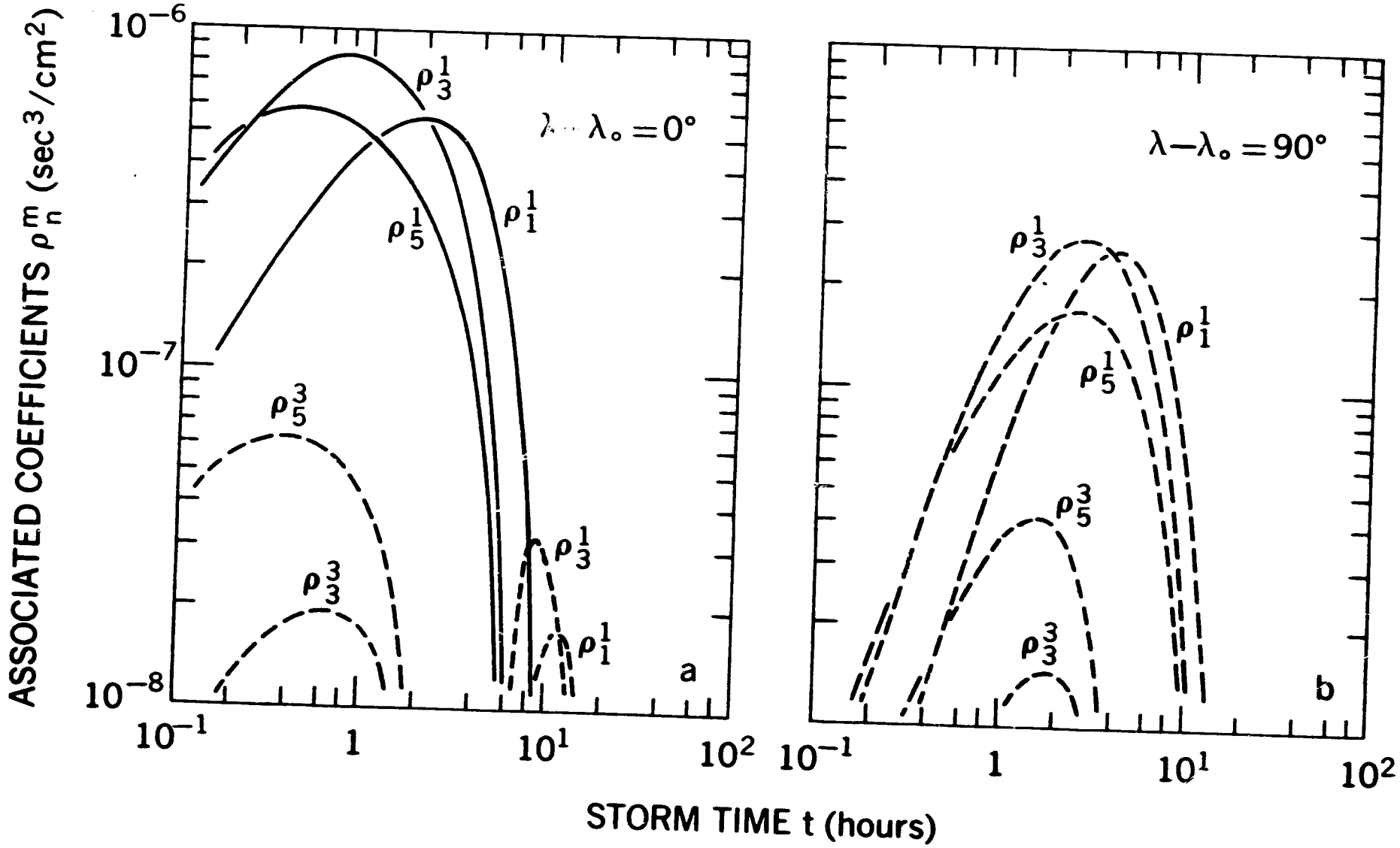

Figure 6. Spherical components $\rho_n^m P_n^m$ ($m > 0$) versus storm time t calculated at the equator ($\varphi = 0°$). Solid lines indicate positive values, dashed lines indicate negative values.

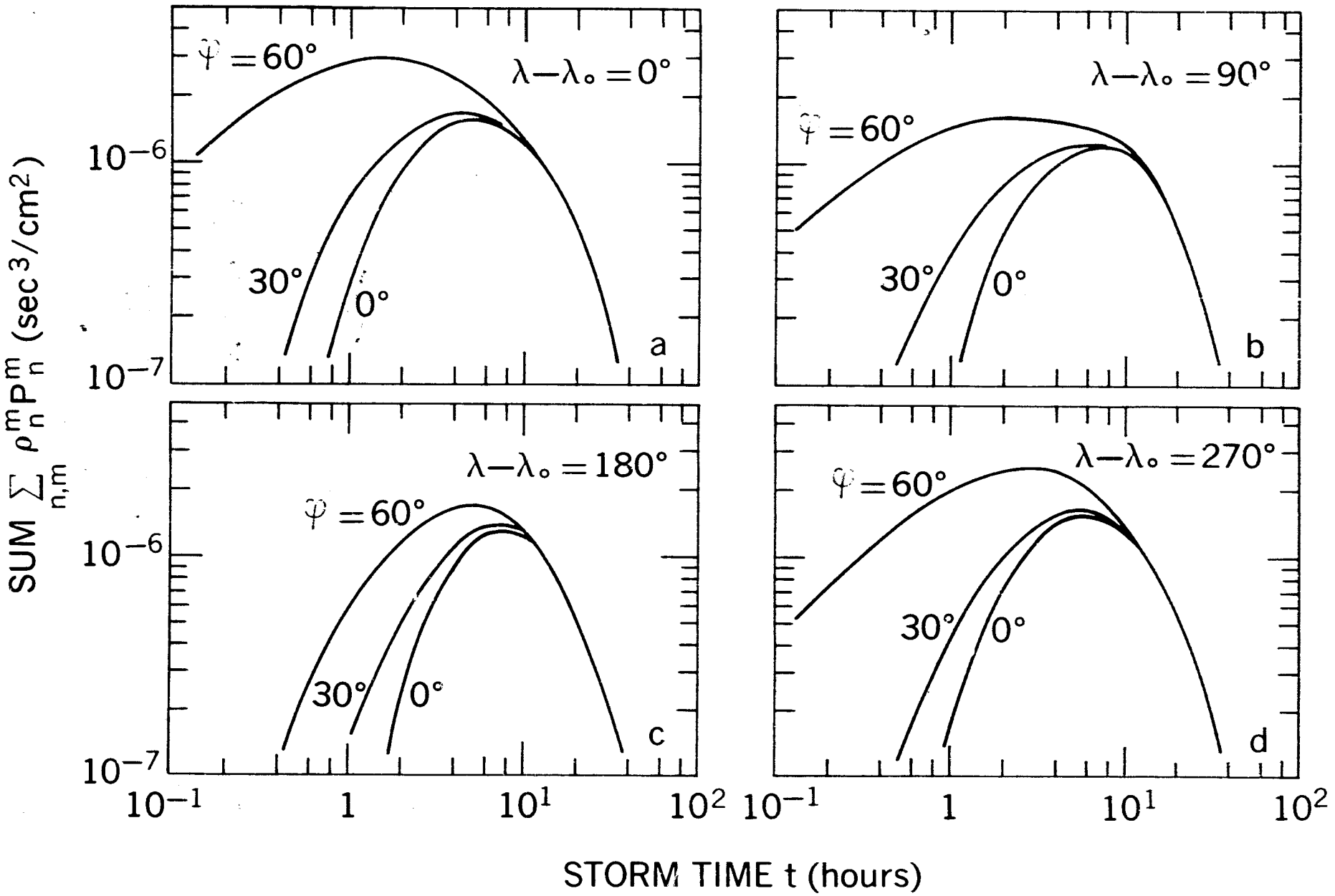

Figure 7. Sum of all components $\Sigma_{n,m} \rho_n^m P_n^m$ versus storm time t for three different latitudes φ and four different longitudes $\lambda - \lambda_0$.

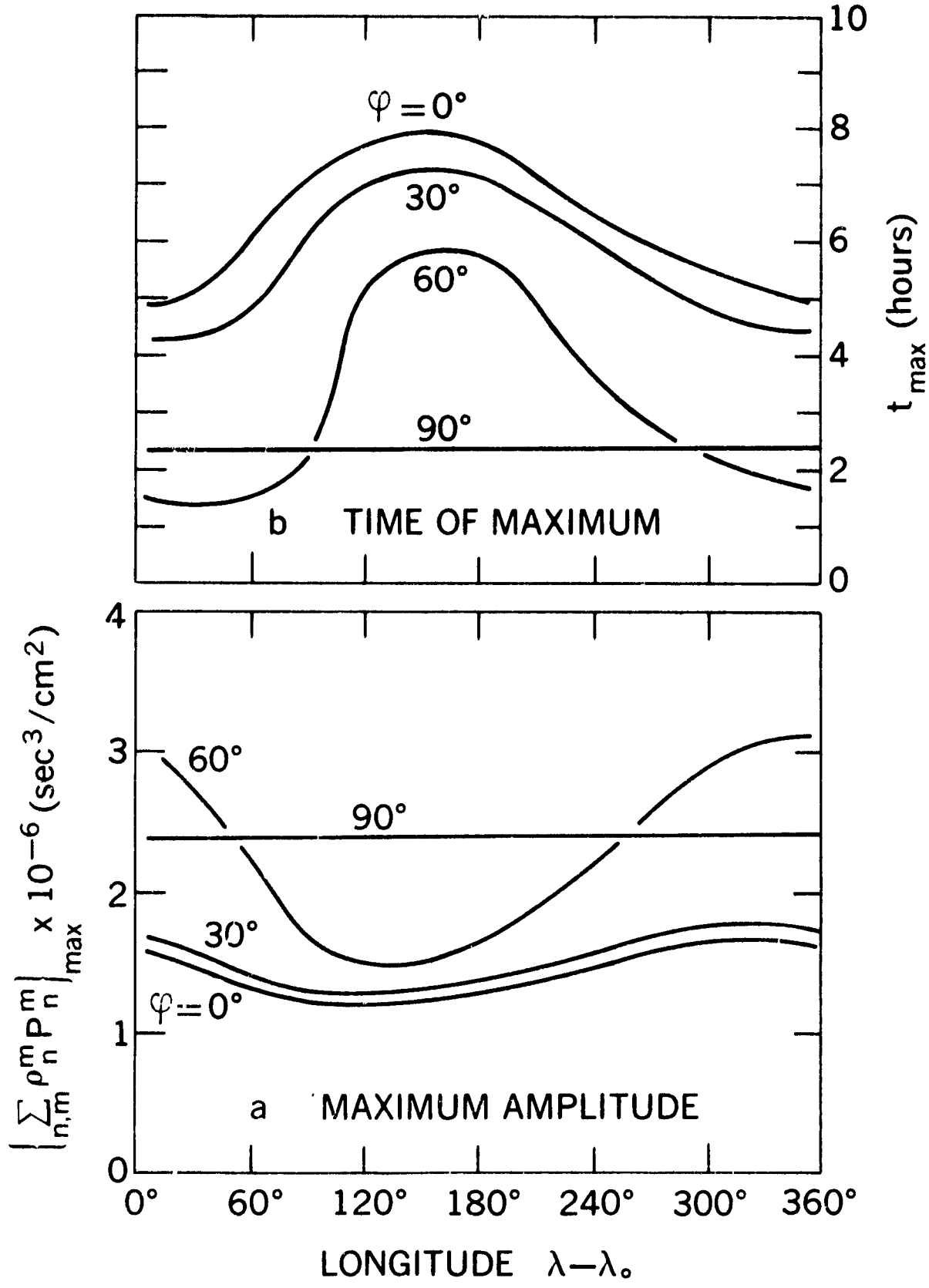

Figure 8. Maximum amplitudes (Fig. 8a) and maximum times (Fig. 8b) taken from Fig. 7 versus longitude $\lambda - \lambda_0$ for four different latitudes φ